THE ASTROPHYSICAL JOURNAL, 444:787–795, 1995 May 10

AN X-RAY AND OPTICAL STUDY OF THE INTERACTION OF THE CYGNUS LOOP SUPERNOVA REMNANT WITH AN INTERSTELLAR CLOUD[1]

JAMES R. GRAHAM,[2,3] N. A. LEVENSON,[2] J. J. HESTER,[4] J. C. RAYMOND,[5] AND R. PETRE[6]
Received 1994 July 7; accepted 1994 November 17

ABSTRACT

We have used the *ROSAT* high-resolution imager and optical emission line data to study the structure of a bright optical knot on the southeastern rim of the Cygnus Loop supernova remnant. This knot has been identified as an encounter between the blast wave and a small isolated cloud. The knot appears in projection just behind the blast wave, which is traced by Balmer line filaments which bound the X-ray emission. The knot is a prominent X-ray feature, consisting of a number of filaments which are correlated with the optical line emission. These data permit a detailed view of the blast wave interaction. By combining the optical and X-ray data it is possible to trace the blast wave as a continuous surface from its southern edge around the western side of the cloud that then continues on to the north. The southeastern knot is an indentation on the surface of the blast wave. Thus the southeastern knot is not a small cloud that has been overrun by the blast wave, but the tip of a larger cloud.

Bright X-ray emission is associated with bright radiative filaments. The location of this emission, upstream of the radiative shocks, implies that the enhanced X-rays come from a reverse shock. The presence of a reverse shock is further evidence that the southeastern knot represents an early stage of a blast wave encountering a large cloud.

A consistent picture of the Cygnus Loop as an explosion within a preexisting cavity is emerging. These observations agree with that picture.

Subject headings: ISM: individual (Cygnus Loop) — supernova remnants — X-rays: ISM

1. INTRODUCTION

Supernova explosions are one of the basic processes which determine the physical and chemical state of the interstellar medium. In an inhomogeneous medium, the interaction of the supernova blast wave with clouds plays a central role. Consequently, observations of the interaction of a blast wave with interstellar clouds form the empirical basis of an accurate understanding of the evolution of supernova remnants and how they shape the interstellar medium. Several authors have discussed the interaction of a blast wave with a cloud in a theoretical context (e.g., McKee & Cowie 1975; Spitzer 1982; Heathcote & Brand 1983; Bedogni & Woodward 1990; Stone & Norman 1992; Klein, McKee, & Colella 1994). Observations show that the expansion of supernova remnants is a complex phenomenon. Interpretation of the data and comparison with models are often frustrated by the projection of multiple emission regions along the line of sight.

There are two contradictory paradigms describing the interaction of a blast wave and the interstellar medium at the edge of a "middle-aged" supernova remnant (SNR) such as the Cygnus Loop. One proposal (e.g., McKee & Cowie 1975) emphasizes the importance of evaporation of small clouds that are engulfed by the passing blast wave. In this view the frequently observed correlation between optical emission and X-ray emission is attributed to thermal evaporation of the clouds into which radiative shocks are being driven. This model has been applied to the X-ray emission from a number of SNRs including the Cygnus Loop (Ku et al. 1984; Charles, Kahn, & McKee 1985) and Puppis A (Petre et al. 1982), and to the optical emission from the Cygnus Loop (Fesen, Blair, & Kirshner 1982).

A second class of models emphasizes that clouds are generally large compared to the physically important scales ($\gtrsim$ few $\times 10^{16}$ cm) for gasdynamic and radiative processes behind the shock. This model characterizes the boundary of an SNR as a large-scale coherent shock marking a sharp division between the interior and exterior of the remnant. This second view has been developed in considerable detail (Hester, Parker, & Dufour 1983; Hester & Cox 1986; Hester 1987; Raymond et al. 1988; Hester & Raymond 1988; Graham et al. 1991b; Graham, Wright, & Geballe 1991a; Hester, Raymond, & Blair 1994). This picture has been very successful in describing a wide range of observational data, including morphological differences among optical and infrared emission lines, discrepancies between steady-flow shock model calculations and observed UV and optical line ratios, spatially resolved velocity profiles of emission lines, and radio surface brightness and polarization data.

The *Einstein* X-ray data for the eastern region of the Cygnus Loop are discussed in detail by Hester & Cox (1986), who show that thermal evaporation fails to account for either the X-ray surface brightness or the relationship between X-ray and optical emission in the region studied. They found that bright X-ray emission is localized in a relatively thin zone immediately behind radiative shocks and that the brightness of the X-ray emission is anticorrelated with the time since the shock-cloud encounter. This is at odds with the evaporative descrip-

[1] Based in part on observations made at the Palomar 60 inch telescope, which is operated jointly by the California Institute of Technology and the Carnegie Institution of Washington.

[2] Astronomy Department, University of California, Berkeley, CA 94720.
[3] Alfred P. Sloan Research Fellow.
[4] Department of Physics and Astronomy, Arizona State University, Tempe, AZ 85287-1504.
[5] Harvard-Smithsonian Center for Astrophysics, 60 Garden Street, Cambridge, MA 02138.
[6] Goddard Space Flight Center, Code 666, Greenbelt, MD 20771.

tion, which predicts that the X-rays should be brighter in the vicinity of clouds that have been exposed to the hot interior of the remnant for a longer period of time. In contrast, Hester & Cox found that a combination of higher postshock density and higher pressures due to blast-wave–cloud encounters explains the X-ray and optical data in a very straightforward way. X-rays are bright in the vicinity of a young radiative shock, primarily because it is here that the blast wave is rapidly decelerating, leading to reflected shocks and other transient increases in density and pressure in the hot postshock gas.

The recent discovery of an isolated cloud in the Cygnus Loop, which may have been engulfed by the blast wave, provides an excellent opportunity to study blast-wave–cloud interactions. Fesen, Kwitter, & Downes (1992) have presented optical emission-line imaging of a small (2′ × 4′) knot in the southeastern region of the Cygnus Loop and proposed that it has been completely overrun by the blast wave. The Balmer line filaments seen in projection ahead of the knot (i.e., further from the center of the remnant) show morphologies highly reminiscent of numerical calculations of shock-cloud encounters. These include structures interpreted as complete shock front reestablishment following cloud passage, a cusplike feature along the symmetry axis associated with the Mach disk, and streamers of gas stripped from the main body of the cloud. Closer to the center of the remnant is another Balmer line filament, which Fesen et al. interpret as a reverse shock.

We present *ROSAT* HRI and optical emission line images of the southeastern knot. The improved *ROSAT* HRI sensitivity and spatial resolution of the telescope, compared to the *Einstein* X-ray observatory, make these observations valuable for exploring the small-scale structure of cloud–blast-wave interactions. Comparison of X-ray with new optical data suggests an alternative explanation at variance with the engulfed cloud model: the initial encounter of the blast wave with a large cloud.

2. OBSERVATIONS

2.1. *X-Ray Observations*

The southeastern knot (R.A. $20^h56^m21^s.2$, decl. 30°23′59″ [J2000]) was observed with the *ROSAT* HRI for 18,965 s on 1991 December 6–10. The *ROSAT* HRI combines high sensitivity in the 0.1–2.5 keV range (about a factor of 3 better than the *Einstein* HRI; Zombeck et al. 1990) and high spatial resolution ($\theta_{80} \simeq 4''$; Aschenbach 1988). The measured FWHM of the point-spread function is 6″ on-axis, increasing to 30″ at the edge of the field. The useful field of view of the HRI is about 30′ × 30′. The data presented here have been smoothed to FWHM = 16″. Figure 1 shows a gray-scale display of the southeastern knot field.

2.2. *Optical Observations*

Observations of the Cygnus Loop were obtained in 1986 August using the wide-field prime-focus universal extragalactic instrument (PFUEI) reimaging camera on the Palomar 60 inch (1.5 m) telescope. This system uses a Texas Instruments 800 × 800 pixel CCD to record an image of 16′ × 16′ at f/1.66. Images were obtained through a 15 Å Hα filter (Fig. 2 [Pl. 29]),

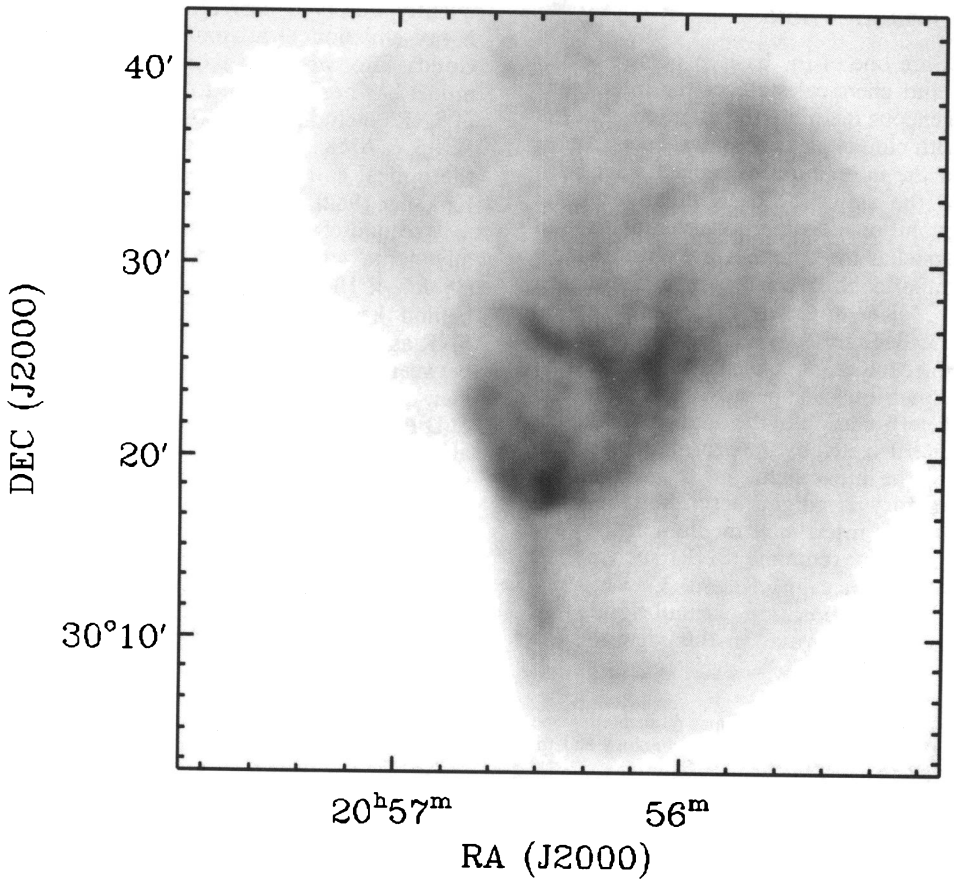

FIG. 1.—*ROSAT* HRI X-ray image of the Cygnus Loop southeastern knot. The data have been smoothed to yield a resolution of 16″. The gray scale is linear with white mapped to 0.0 and black to 0.10 counts s^{-1} $arcmin^{-1}$.

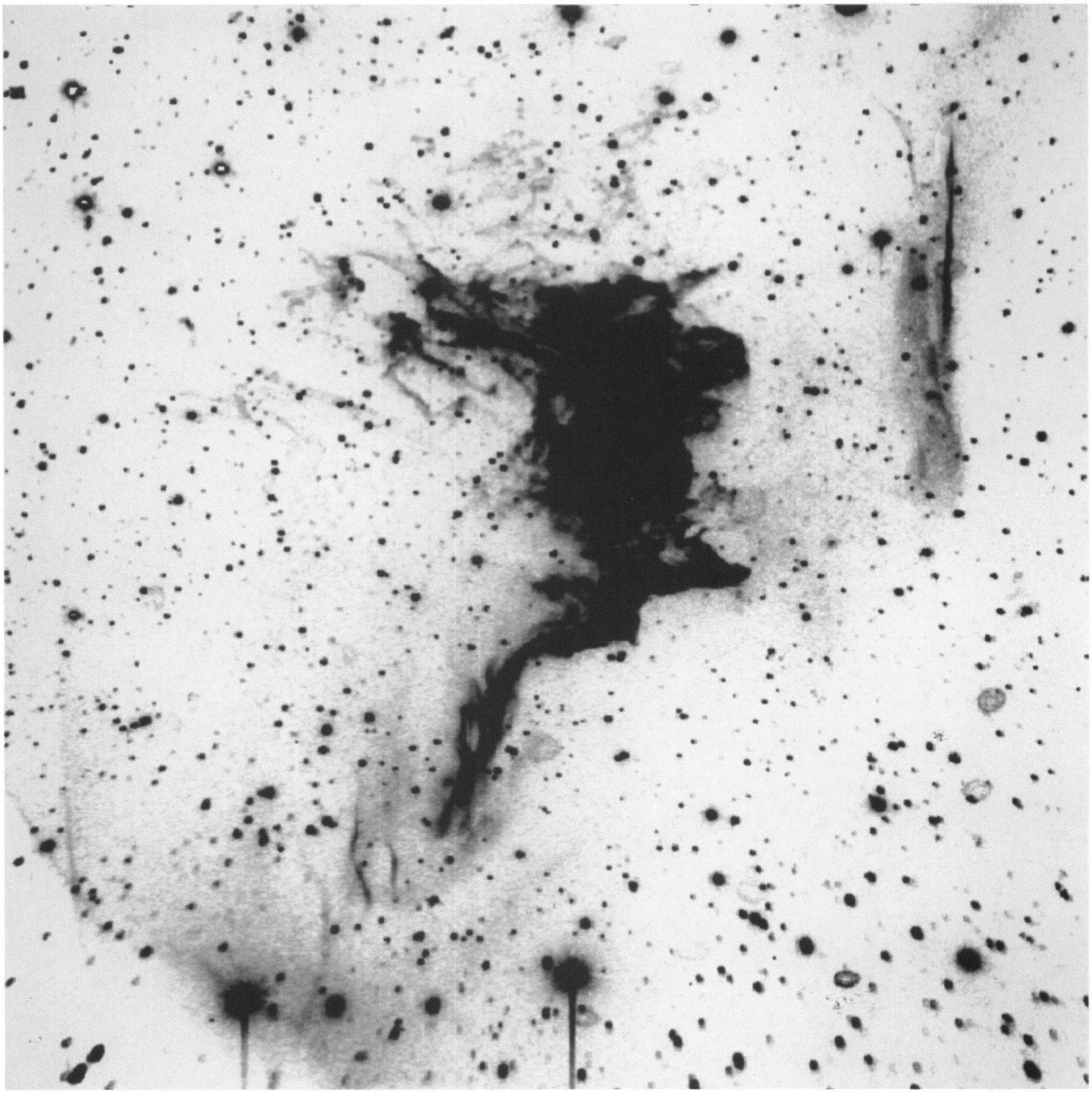

FIG. 2.—Palomar 60 inch wide PFUEI Hα image of the Cygnus Loop southeastern knot. The field of view is 16′ × 16′. North is at the top, and east to the left.

GRAHAM et al. (see 444, 788)

a 32 Å [O III] λ5007 filter (Fig. 3 [Pl. 30]), and a 35 Å [S II] λ6731/λ6716 filter (Fig. 4 [Pl. 31]). The CCD data were bias subtracted using an overscan of the serial registers and flattened using dome flats taken at the beginning and end of the night.

Additional observations were made at the 40 inch (1.0 m) telescope at Lick Observatory with a Ford 2048 × 2048 CCD on 1993 August 26–27. The CCD was used with 2 × 2 on-chip binning to yield an effective pixel size of 0".36. Images were obtained with filters designed to cover Hα (λ6563, $\delta\lambda = 45$ Å), [O III] (λ5030, $\delta\lambda = 75$ Å), and [S II] (λ6737, $\delta\lambda = 90$ Å).

3. RESULTS

3.1. *Optical Emission Line Imaging*

Optically, the southeastern knot exhibits a chaotic structure. The radiative shocks, i.e., those traced in Hα, [O III], and [S II], do not exhibit the characteristic large-scale filamentary structure typical of the bright radiative shock in the northeast of the remnant (e.g., Hester 1987). However, there are some short filaments, and comparison of the Hα, [O III], and [S II] images of the southeastern knot shows clear stratification of the optical line emission typical of other shocked regions in the Cygnus Loop. Across the main body of the optical knot, Balmer-dominated emission is seen in projection in front (to the east) of [O III]-bright shocks with incomplete cooling and recombination regions, which in turn are seen in projection in front of shocks which show strong emission in [S II]. This type of emission-line morphology is discussed within the context of other blast-wave–cloud encounters in the Cygnus Loop by Hester (1987, Figs. 7 and 8), who interpreted emission-line stratification in terms of the progression of shock velocity, preshock density, and the column depth accumulated by the shock with apparent distance behind the projected leading edge of a shocked cloud.

The southeastern knot is not symmetrical. A bright well-defined Balmer-dominated filament extends from the southern end of the knot, while in the northeast the cloud trails off into a broken set of filaments including both Balmer-dominated and incomplete [O III] filaments, as well as some faint [S II] emission. There is also a north-south asymmetry in the strength of [S II] emission, with a complex of shocks with strong [S II] but fairly weak [O III] extending to the northwest of the knot.

Very faint Balmer-dominated emission can be seen throughout the field, including a number of filaments running roughly east-west located 3′–5′ to the east of the northern portion of the knot. A bright Balmer-dominated filament lies just to the west of the southeastern knot. This filament appears to be a section of the blast wave seen in projection behind the cloud.

3.2. *X-Ray Images*

The southeastern knot appears as a prominent feature in the *ROSAT* HRI image and corresponds to a region of well-defined and well-resolved X-ray filaments superimposed on a region of roughly uniform emission (Fig. 1). The thickness of these filaments is typically FWHM $\simeq 60''$, or $\sim 7 \times 10^{17}$ cm, assuming a distance of 770 pc (Minkowski 1958). These filaments are located at the apex of a large indentation of the X-ray shell. The location of the knot, and its relationship to the large-scale structure of the Cygnus Loop, is shown in Figure 5, which shows the *Einstein* X-ray image of the entire remnant.

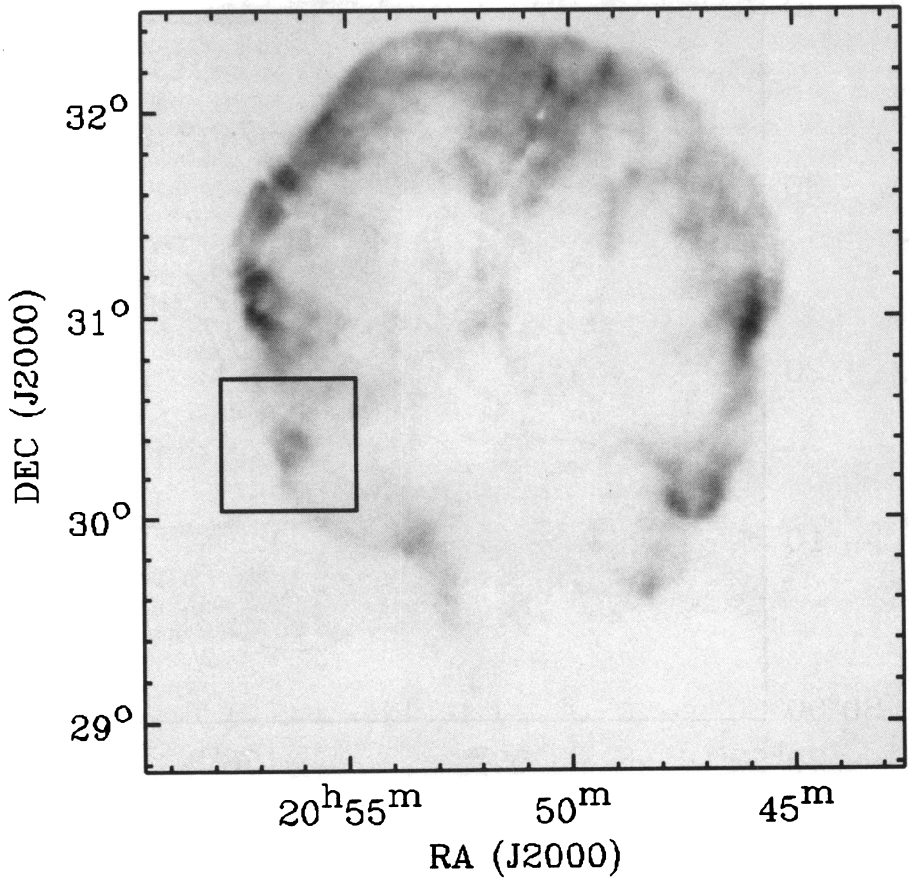

FIG. 5.—*Einstein* IPC (0.1–4.5 keV) image of the Cygnus Loop (Seward 1990). The box indicates the location of the *ROSAT* HRI field shown in Fig. 1.

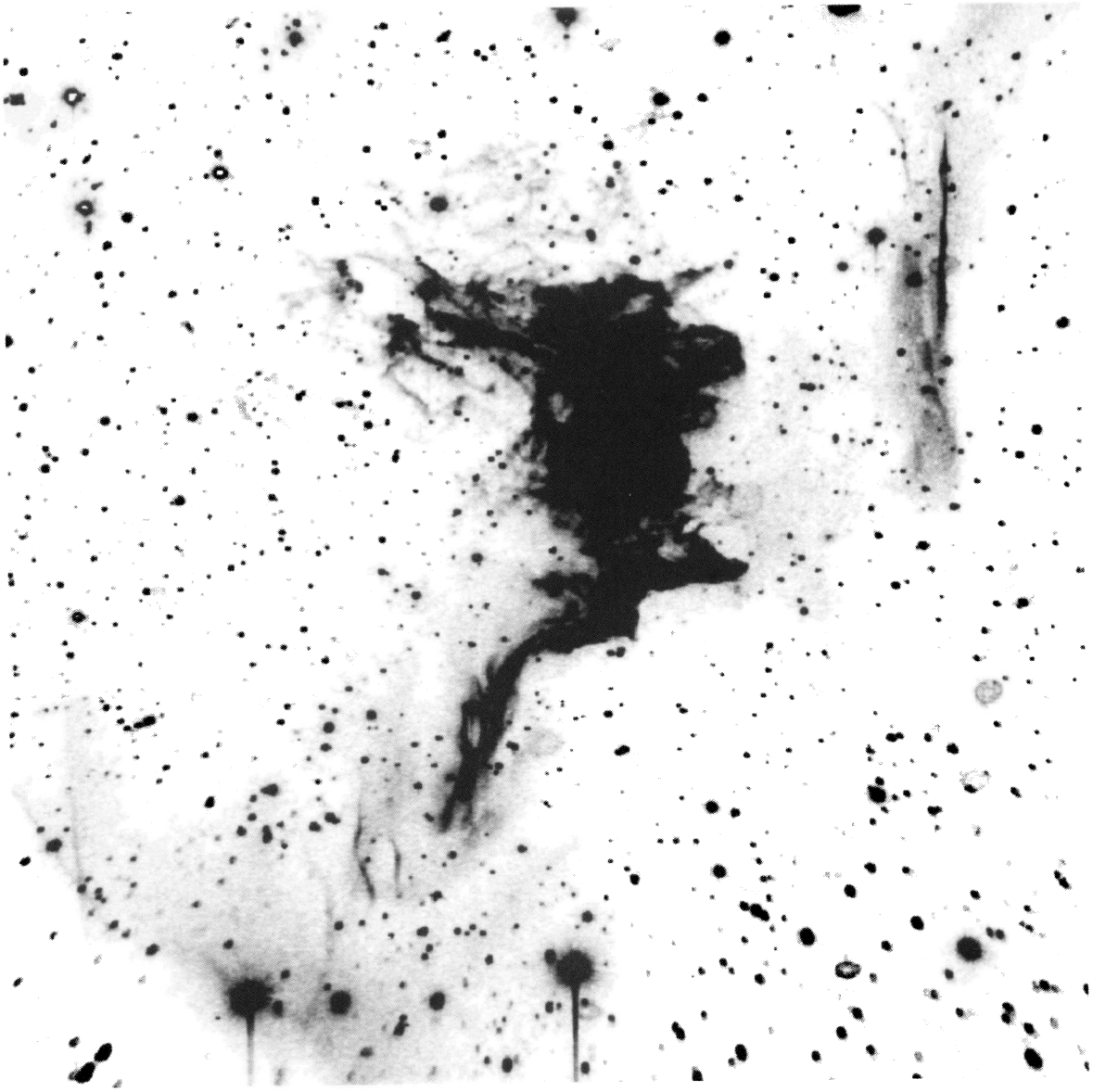

FIG. 2.—Palomar 60 inch wide PFUEI Hα image of the Cygnus Loop southeastern knot. The field of view is 16′ × 16′. North is at the top, and east to the left.

GRAHAM et al. (see 444, 788)

PLATE 30

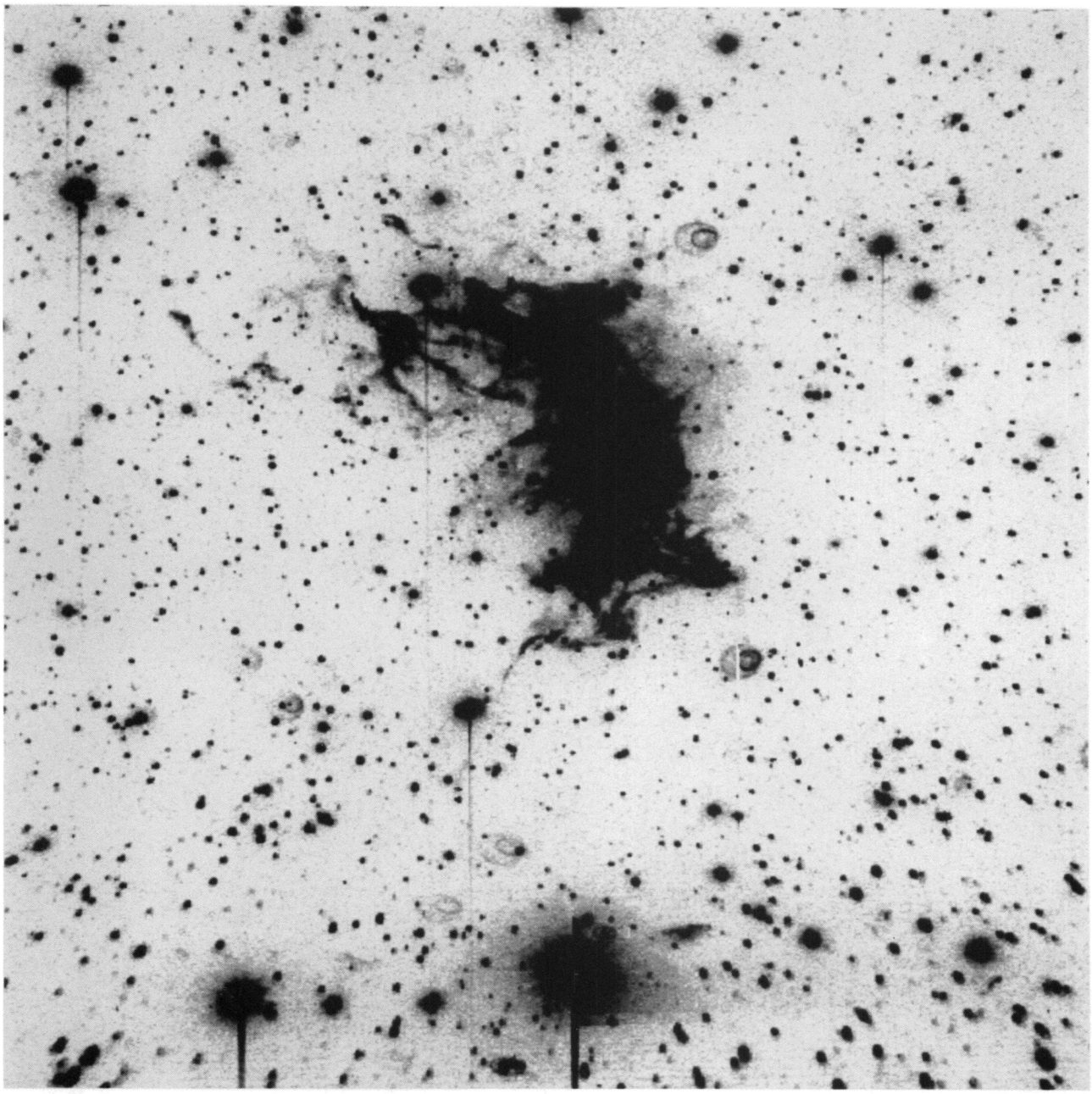

FIG. 3.—Palomar 60 inch wide-field PFUEI [O III] image of the Cygnus Loop southeastern knot. The field of view is 16′ × 16′. North is at the top, and east to the left.

GRAHAM et al. (see 444, 789)

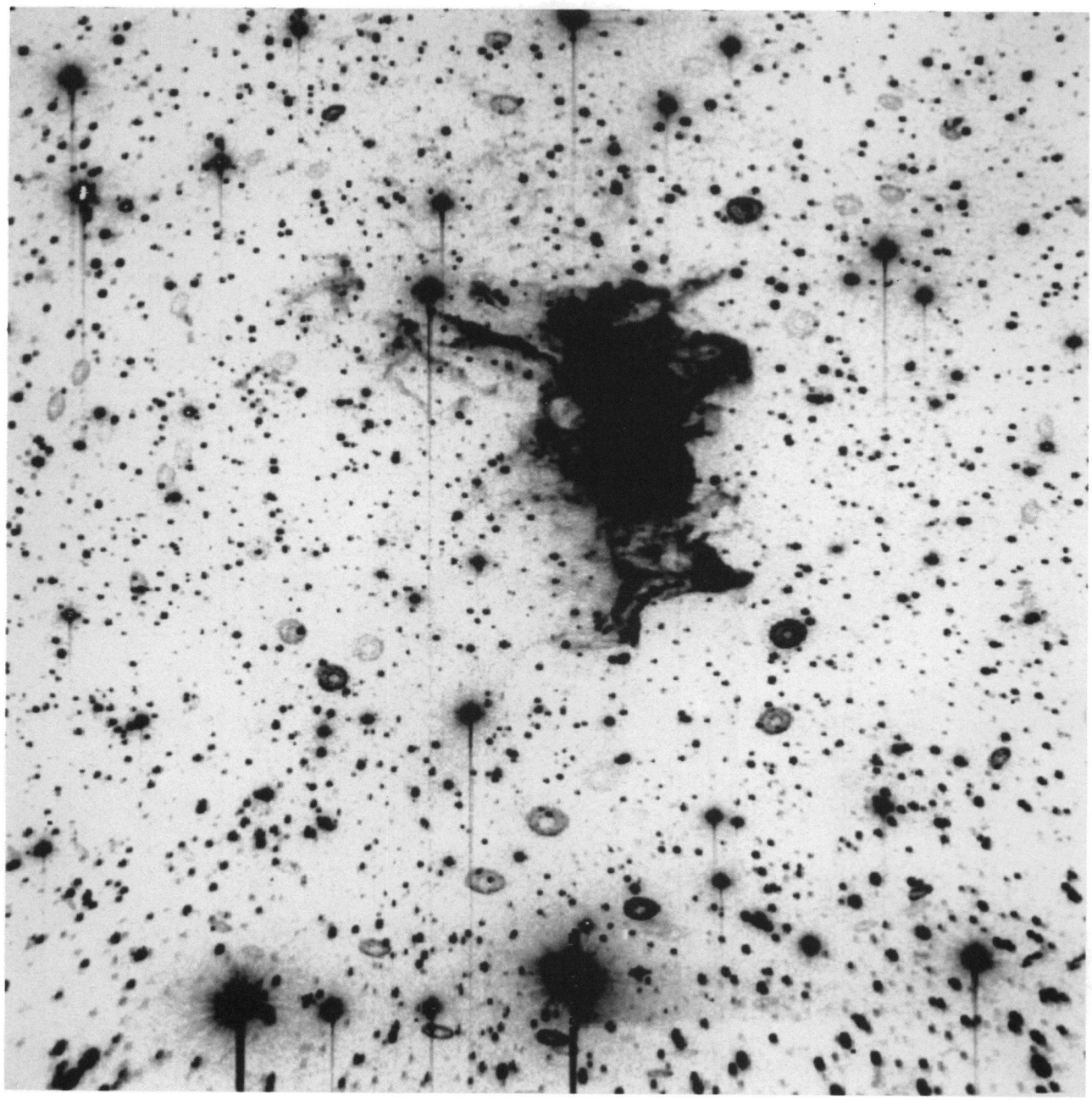

FIG. 4.—Palomar 60 inch wide-field PFUEI [S II] image of the Cygnus Poop southeastern knot. The field of view is 16′ × 16′. North is at the top, and east to the left.

GRAHAM et al. (see 444, 789)

The southern section of the X-ray emission is prominent, sharp, and limb-brightened, while the northern portion is fainter and consists of a more gradual edge. The southern section shows the sharpest X-ray structure, which is resolved with an observed half-width at half-maximum of $\simeq 40''$. The X-ray edge is similar to that seen to the northeast of the Cygnus Loop, and on the eastern limb (Hester, Raymond, & Blair 1994; Hester & Cox 1986). The sharpness of this feature, and its association with faint Balmer line filaments (Fesen et al. 1992), confirms that this edge delineates the blast wave.

The differences between the X-ray emission from the northern and southern sections of the blast wave may be due to a combination of varying density and different projections of the blast wave. The brightness and sharpness of the southern portion suggests that a substantial column of the blast wave is seen very close to tangency to the line of sight. The pronounced curvature of the northern section, as projected onto the plane of the sky, suggests substantial three-dimensional curvature of the blast wave here. This implies only a limited potential for limb brightening.

There is good correlation between X-ray and optical emission. Figure 6 shows contours of X-ray emission overlayed on the Hα image of Fesen et al. (1992). Generally, there is a one-to-one correspondence between bright X-ray and optical filaments. The clearest correlation is the association along the leading edge of the blast wave. The northern and southern sections of the blast wave consist of X-ray emission bounded on the east by sharp Balmer-dominated filaments. No X-ray emission is detectable beyond the bounding Balmer-dominated filament above 1% (3 σ) of the peak level.

The relationship between the X-ray emission and radiative filaments is more complex. One group of X-ray filaments is located immediately behind (to the west and northwest of) the bright radiative shocks which delineate the main body of the southeastern knot. The X-ray filament associated with the northern end of the knot extends further to the northeast than the optical filaments. The brightest X-ray feature in the field is a knot of emission located at the southeastern end of the Balmer-dominated filament that originates at the southern end of the optical knot.

There are several regions where the correlation between optical and X-ray emission is poor. The region of X-ray emission running east-southeast to west-northwest across the field to the south of the optical knot is one example; another is the southern portion of the optical knot that is conspicuous for its *lack* of corresponding X-ray emission.

4. THE SOUTHEASTERN KNOT AS A CLOUD–BLAST-WAVE INTERACTION

The presence of bright optical radiative filaments in the southeastern knot indicates that this is a region where the blast wave is running into a localized region of higher density. Fesen et al. (1992) present wide-field Hα images of the eastern portion of the Cygnus Loop which includes the southeastern knot. The southeastern knot appears in projection just behind (i.e., to the west of) the faint Balmer line filaments. Fesen et al. interpret

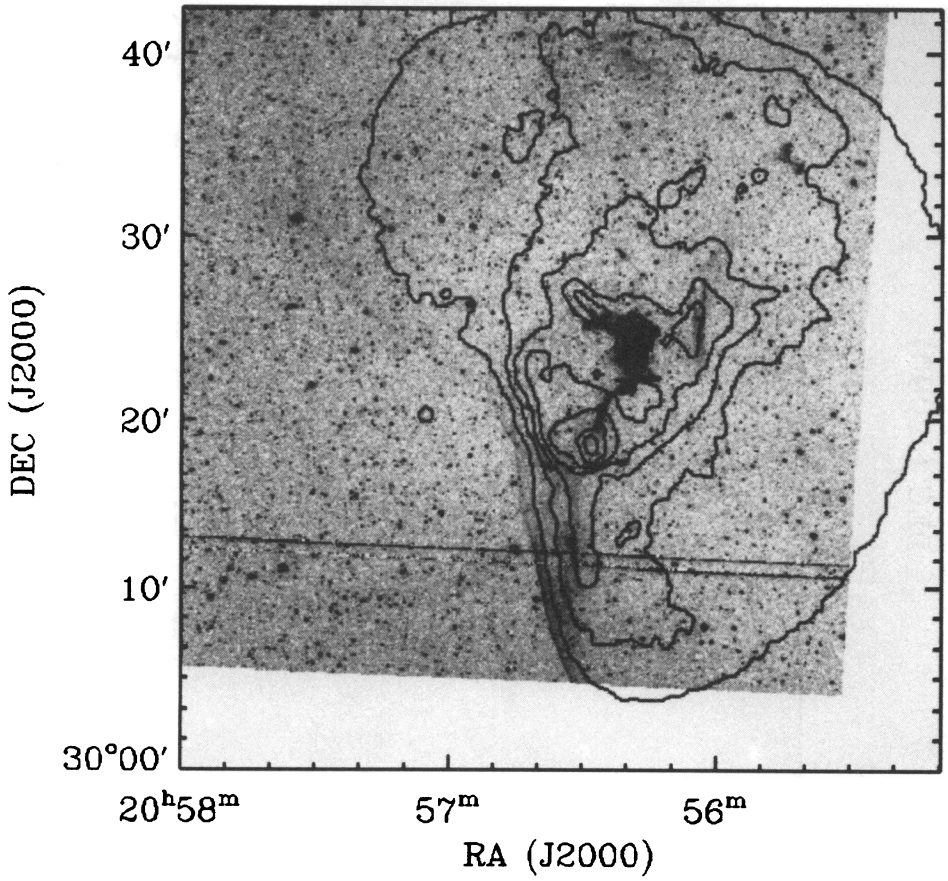

FIG. 6.—Contours of X-ray emission overlaid on the Hα image of Fesen et al. (1992). The contour levels are 0.01, 0.02, 0.04, 0.05, 0.06, 0.08, and 0.09 counts s^{-1} $arcmin^{-1}$.

the optical emission line morphology as a small isolated interstellar cloud which has suffered a recent collision with the blast wave. In this view the blast wave has diffracted around the cloud, and has reestablished ahead of the cloud. Figure 7 sketches the configuration envisioned by Fesen et al. Based on these new observations we modify the interpretation and suggest that the southeastern knot is part of a much larger cloud which has not yet been engulfed. Consequently, the southeastern knot represents the early stages of an encounter between a cloud and the blast wave.

4.1. *Optical and X-Ray Morphology of the Blast Wave*

The new optical and X-ray observations reveal several difficulties with the engulfed cloud model. Both the overall shape of the blast wave inferred from these data and several features of the optical and X-ray emission associated with the southeastern knot are inconsistent with an engulfed cloud.

Inspection of the digital data from Fesen et al. (1992) at high contrast leaves one with the distinct impression that the Balmer line filaments form an almost continuous surface, from their projected eastern extent around the *western* side of the cloud, with the radiative knot forming an identation on this surface. This morphology indicates that the blast wave has not overrun the cloud. The asymmetry of the optical and X-ray emission associated with the southeastern knot suggests that the cloud must be nonspherical. The configuration is illustrated in Figure 8. The bright radiative shocks of the southeastern knot may trace a protrusion on the surface of the cloud, such as an elephant-trunk structure which formed in the progenitor's H II region, marking the location where the density is high enough, and the interaction old enough, for the blast wave to develop a postshock cooling and recombination zone.

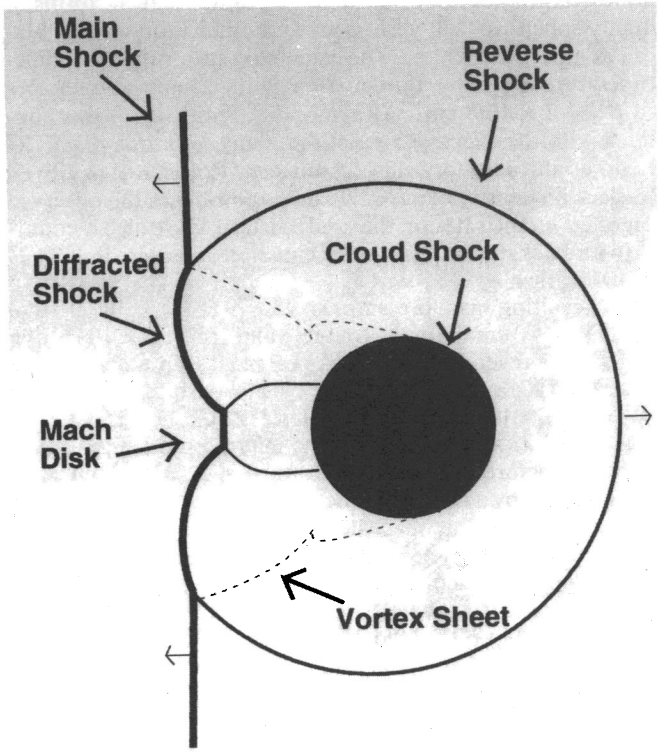

FIG. 7.—Sketch of the interaction of a blast wave and an interstellar cloud based on calculations of Stone & Norman (1992) and Klein et al. (1994). The blast wave is propagating from the right to left and has engulfed the cloud. Some of the features identified by Fesen et al. (1992) are labeled.

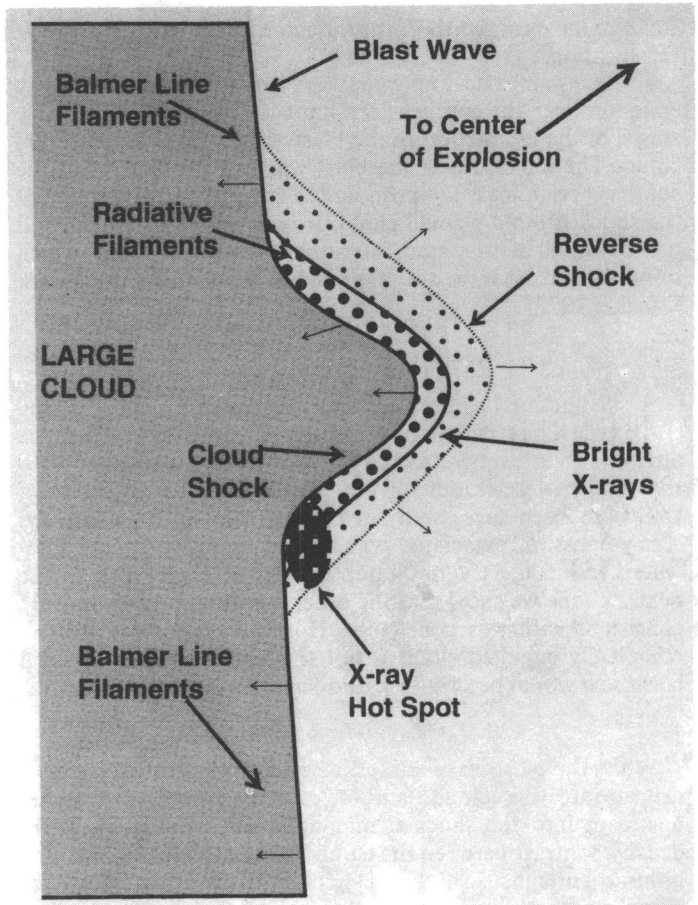

FIG. 8.—Configuration of the southeastern knot inferred from combined X-ray and optical data. In contrast with the picture sketched in Fig. 7, the southeastern knot is not an engulfed cloud, but a protrusion on a larger structure.

The continuation of the southern section of the blast wave up and around the back of the cloud is apparent, but the connection of the northern end of the knot to the blast wave cannot be discerned in Balmer line emission alone. But, when the cloud is viewed simultaneously in the optical and X-rays, the funnel-shaped indentation in the blast wave becomes more apparent (Fig. 6). By following optical and X-ray emission it is possible to trace the shock from the northern and southern edges of the cloud to the current projected edge of the blast wave. Specifically, the connection to the northern section of the blast wave can be followed along the bright X-ray filament that delineates the northern tip of the optical knot.

It is important to view the southeastern knot within the context of the large-scale structure of the Cygnus Loop. The *Einstein* IPC image of the Cygnus Loop (Fig. 5) (Seward 1990) shows that the southeastern knot is located at the apex of an indentation in the X-ray shell with a size of about 30′. This observation is independent evidence that the southeastern knot is associated with a structure which is much larger than the 2′ × 4′ optical knot. When a blast wave interacts with an isolated cloud, the main shock is diffracted over a scale comparable to the diameter of the cloud (Stone & Norman 1992; Klein et al. 1994; cf. Fig. 7, which is based on these calculations). The knot, visible in radiative shock tracers, is too

small to have caused the large indentation in the blast wave at this location.

The *Einstein* data imply that the bright optical and X-ray emission near the southeastern knot is the result of the early stages of the interaction of the blast wave with a large ($\simeq 30'$) cloud. The curvature of the blast wave in the vicinity of the southeastern knot is too pronounced to be due to diffraction of the shock around a small cloud. It is plausible that the cloud has a gradual density gradient, rather than a sharp edge, which refracts the blast wave as it approaches the cloud (cf. McKee & Ostriker 1977).

4.2. *X-Ray Emission from a Reverse Shock*

A distinctive feature of the southeastern knot is the enhanced X-ray emission upstream of the cloud, which we attribute to a reverse shock. The overpressure associated with the sudden deceleration of the blast wave when it strikes a cloud has been successfully invoked to explain the enhanced X-ray emission associated with bright radiative shocks elsewhere within the Cygnus Loop (Hester & Cox 1986). In the next sections we show that the observations are quantitatively consistent with this conjecture. Hot gas evaporated from a completely engulfed cloud is not the source of this emission because it would be swept *downstream* with the shocked gas.

4.2.1. *Formation of a Reflected Shock*

When the blast wave strikes a cloud, a transmitted shock is driven into the cloud, and a reflected shock propagates upstream into the shocked intercloud gas (cf. Fig. 7). If the density contrast between the cloud and the intercloud medium is large enough, then the velocity initially imparted to the cloud material is small, and the cloud can be treated as an incompressible obstacle. So long as the flow is approximately one-dimensional the ratio of the pressure behind the incident shock, p_1, to that behind the reflected shock, p_2, is

$$\frac{p_2}{p_1} = \frac{3\gamma - 1}{\gamma - 1}$$

for a strong shock, where γ is the ratio of specific heats. If $\gamma = 5/3$, then $p_2/p_1 = 6$ (Spitzer 1982). The reflected shock moves outward and weakens because of divergence. Steady flow past the cloud is set up in a time comparable to the time for sound in the shocked intercloud medium to travel round the cloud. If $t_{ic} = 2a_0/v_b$ is the time for the blast wave (velocity v_b), to sweep over the cloud (initial radius a_0), then steady flow is achieved in a time of order $\frac{1}{2}t_{ic}$, and the reflected shock evolves into a standing shock if the flow of gas behind the blast wave is supersonic with respect to the cloud boundary. The pressure between the position of the reverse shock and the stagnation point ranges over (2–3.15) p_1 for an incompressible cloud (Landau & Lifshitz 1987; McKee & Cowie 1975).

4.2.2. *Morphology of the Reverse Shock*

Much of the X-ray emission in the immediate vicinity of the cloud appears to be physically associated with the cloud because it is correlated with bright radiative filaments. This morphology is consistent with the view that the bright radiative filaments are the cloud shock and the enhanced X-ray emission is due to a reverse shock. The presence of bright Hα, [S II], and [O III] emission from the radiative filaments implies a cloud shock speed is ≈ 100 km s^{-1}. The blast wave speed is in the range 200–400 km s^{-1} (Ku et al. 1984; Hester et al. 1994), so that pressure balance requires that the cloud's density contrast be $\rho_c/\rho_{ic} \approx 4$–16. The lower end of the range of blast wave velocities, 200 km s^{-1}, is derived from Balmer line filaments where the shock has run into higher than average density gas. Therefore, $\rho_c/\rho_{ic} \approx 10$ is probably a good characteristic number. For a cloud with such a small density contrast, the flow of the shocked intercloud gas is not supersonic relative to the cloud boundary, and the bow shock rapidly weakens into a bow wave (McKee & Cowie 1975; Klein et al. 1994). Thus, the reverse shock is a transient feature which dissipates rapidly once the cloud is engulfed and accelerated. If we ascribe the conspicuous X-ray emission associated with the southeastern knot to a reverse shock, then we are forced to surmise that blast wave encounter is at an early stage, before the cloud has been engulfed, and that $t \ll \frac{1}{2}t_{ic}$. Therefore, the large cloud depicted in Figure 8 is probably a better representation of the circumstances than the engulfed cloud shown Figure 7.

4.2.3. *Pressure in the X-Ray–emitting Gas*

We can estimate the pressure of the X-ray–emitting gas from the HRI data as follows. The *ROSAT* HRI has insufficient energy resolution to enable us to determine the temperature of the emitting gas. However, X-ray spectroscopy indicates that the temperature of the X-ray–emitting gas in the Cygnus Loop is $T_e = (2\text{–}4) \times 10^6$ K, with the brightest regions having $T_e \simeq 2 \times 10^6$ K (Ku et al. 1984; Charles et al. 1985). The absorbing column derived from X-ray observations is $N_H = (2.6\text{–}4.4) \times 10^{20}$ cm^{-2} (Charles et al. 1985). *ROSAT* proportional counter observations of the X-ray bright region to the north of the southeastern knot indicate values at the lower end of this range, and therefore we assume $N_H = 2 \times 10^{20}$ cm^{-2} (Curiel et al. 1995). The volume of the emitting region surrounding the southeastern knot is calculated assuming that it forms a roughly spherical shell with inner and outer radii of 160″ and 320″, at a distance 770 pc. The calculated spectrum of a single-temperature optically thin plasma with cosmic abundances and $N_H = 2 \times 10^{20}$ cm^{-2} (Raymond & Smith 1977) was convolved with the effective area of the X-ray telescope plus HRI (David et al. 1993) to yield a count rate. For $T_e = 2 \times 10^6$ K, and electron density of $n_e = 1.9$ cm^{-3} reproduces the observed integrated count rate for the southeastern knot of 2.8 counts s^{-1} (with background blast wave emission subtracted). If $T_e = 4 \times 10^6$ K, then $n_e = 1.3$ cm^{-3}.

The resulting gas pressure is $P = (9.6\text{–}13) \times 10^{-10}$ dyn cm^{-2}. This is comparable to the value of $\approx 2 \times 10^{-9}$ dyn cm^{-2} for the reverse-shocked XA region (Hester & Cox 1986). Optical and X-ray estimates of the blast wave pressure indicate $P_{BW} = (2\text{–}3) \times 10^{-10}$ dyn cm^{-2} (Hester & Cox 1987; Ku et al. 1984; Hester et al. 1994). Hence the inferred pressure is $\simeq 3$–6 times the pressure behind the blast wave and is consistent with pressurization by a reflected shock (cf. § 4.2.1).

We emphasize that the calculation of the pressure in the X-ray–emitting gas is subject to several uncertainties. Depletion of iron and silicon in grains alters the temperature and ensity estimates somewhat. Because depletion can decrease X-ray emissivity up to a factor of 2, the density estimate may increase by $2^{1/2}$. Depletion also affects the hardness of the X-ray spectrum, leading to an overestimate of the temperature of up to 40%. Taking this into account, the temperature in the region of the southeast cloud is more likely in the range $T_e = (1\text{–}2) \times 10^6$ K, and the density closer to $n_e = 2.7$ cm^{-3}. However, since we are concerned with comparing the pressure in different parts of the Cygnus Loop, inferred mostly from

interpreting X-ray emission, by adopting the same assumptions as previous authors we can expect to minimize errors in calculating the pressure ratio.

4.3. *Evidence for an Engulfed Cloud?*

Several pieces of evidence have been adduced in favor of interpreting the southeastern knot as an engulfed cloud: (1) a Balmer line filament to the west of the cloud is identified as a reverse shock (Fesen et al. 1992); (2) the Balmer line filament which joins the southern end of the knot to the main blast wave resembles material stripped from the cloud by dynamical instabilities in numerical simulations (Fesen et al. 1992); (3) the cusplike morphology of the Balmer line filament to the east of the knot recalls the Mach disk which is formed when the blast wave is reestablished ahead of the cloud. We now explain why none of these stand up to thorough scrutiny.

4.3.1. *A Balmer Line Reverse Shock?*

In § 4.2 we have argued that the enhanced X-ray emission from the southeastern knot is due to a reverse shock. The filament to the west of the knot cannot be the optical counterpart of the reverse shock; it is Balmer-dominated and must be a section of the main blast wave moving into predominantly neutral material. When this filament is viewed at high contrast it exhibits a distinct convex curvature—opposite to that expected for a reverse shock. Part of this filament is sharp—like those at the edge of the remnant which trace the blast wave. However, lower surface brightness emission lies to the east and the west (Fig. 2), suggesting that this filament is a point of inflection of the blast wave. The line of sight to a point of inflection must lie behind the projected edge of the blast wave. X-ray emission is strong near this filament, as it is near the Balmer-dominated filaments which delineate the blast wave to the south of the cloud.

Figure 6 shows that a filament of X-ray emission is associated with the alleged Balmer filament "reverse shock." The X-ray filament has a sharp edge which lies in projection along the eastern side of the Balmer filament. Elsewhere in the field, X-ray emission lies to the west of, and is bounded by, Balmer filaments. The alignment of X-ray and Balmer emission to the west of the bright optical knot, if taken at face value, implies that the shock is traveling from east to west—supporting the interpretation of the optical feature as a reverse shock. While it may seem contrived and artificial, the association of the Balmer line and X-ray filaments must be due to chance. This is because the optical filament is Balmer dominated and must be due to a shock propagating in unshocked, neutral gas. Inspection of Figure 6 shows that the Balmer line emission does not bound the X-ray filament in the same way that is seen at the northern and southern sections of the blast wave. Clearly, the situation to the west of the southeastern knot is complicated, with multiple projections of optical and X-ray emission from the blast wave and X-ray emission from the reverse shock discussed in § 4.2.

4.3.2. *Kelvin-Helmholtz Streamers?*

The optical filaments joining the southern end of the southeastern knot have been interpreted as material stripped off the cloud by dynamical instabilities (Fesen et al. 1992). But these appear as Balmer-dominated filaments, which occur only as the blast wave enters neutral material. Streamers of shocked gas from the cloud would be ionized and thus cannot explain these filaments. The stratification of X-ray, Balmer line, and radiative shock emission extending from the southern end of the southeastern knot is precisely the morphology that Hester (1987) links with the progression of shock velocity, preshock density, and the column depth accumulated by the shock when an SNR blast wave encounters a large cloud. This is also exactly opposite to the most obvious guess at the progression expected for stripped material. There are no applicable calculations, but the material farthest from the cloud has had the longest time to ionize, cool, and recombine. Klein et al. (1994) also point out that the southeastern streamer is not the result of a Kelvin-Helmholtz instability because its orientation is wrong; streamers should be blown back and not be tangential to the shell.

4.3.3. *The Mach Disk?*

Another feature characteristic of an engulfed cloud is the Mach disk that forms behind the cloud when the blast wave converges on itself (Fig. 7). Klein et al. (1994) have identified the kinked Balmer-dominated filaments to the east of the cloud with the Mach disk. Their two-dimensional simulations show that the Mach disk lags behind the undisturbed portions of the blast wave. Therefore, the Mach disk of a three-dimensional cloud, seen in projection on the sky, should appear projected behind the blast wave. To see this consider Figure 7 with the line of sight in the plane of the paper, and imagine viewing the cloud from the top or bottom of the page. This is further demonstrated by the two-dimensional representation of the three-dimensional calculations of cloud–blast-wave interactions by Stone & Norman (1992). Klein et al. counter this objection by arguing that the cloud must be cylindrical, with the long axis oriented along the line of sight. Selection effects may favor clouds which have greater column depth along the line of sight, and an elongated cloud is difficult to rule out.

However, there are two new observations which challenge the identification of the cusplike section of the blast wave with a Mach disk. Deep Hα images reveal that the blast wave is not kinked. Figure 9 shows that the shocks here form an "X," and therefore the shape is due to two separate shocks that are projected along the same line of sight propagating in different directions. Being Balmer dominated, both these shocks must be entering neutral regions. Consequently, this morphology cannot result from two shocks colliding to form a Mach reflection. If these shocks were really intersecting, there would be no preshock neutral hydrogen behind an X-ray–emitting shock to form the interior (western) portions of the "X." These shocks appear to be one projection of the blast wave, say the projection on the far side of the cloud, running from northeast to southwest across the field, crossing the same line of sight as the projection on the near side of the cloud, which extends to the south.

Finally, the Mach disk forms where the diffracted blast wave converges on itself and therefore is the location of the highest pressure around the cloud (cf. Falle & Giddings 1988). Since the soft X-ray emissivity of hot gas is primarily sensitive to pressure (cf. Charles et al. 1985), the putative Mach disk should be the most prominent feature in the *ROSAT* image of the southeastern knot; it is not.

4.3.4. *The X-Ray Hot Spot*

The brightest region in the HRI image is southeast of the cloud, at the southern end of the bright Balmer line filament. If this region of enhanced X-ray emission is also due to a reverse shock, then this implies, as we have suggested above, that the

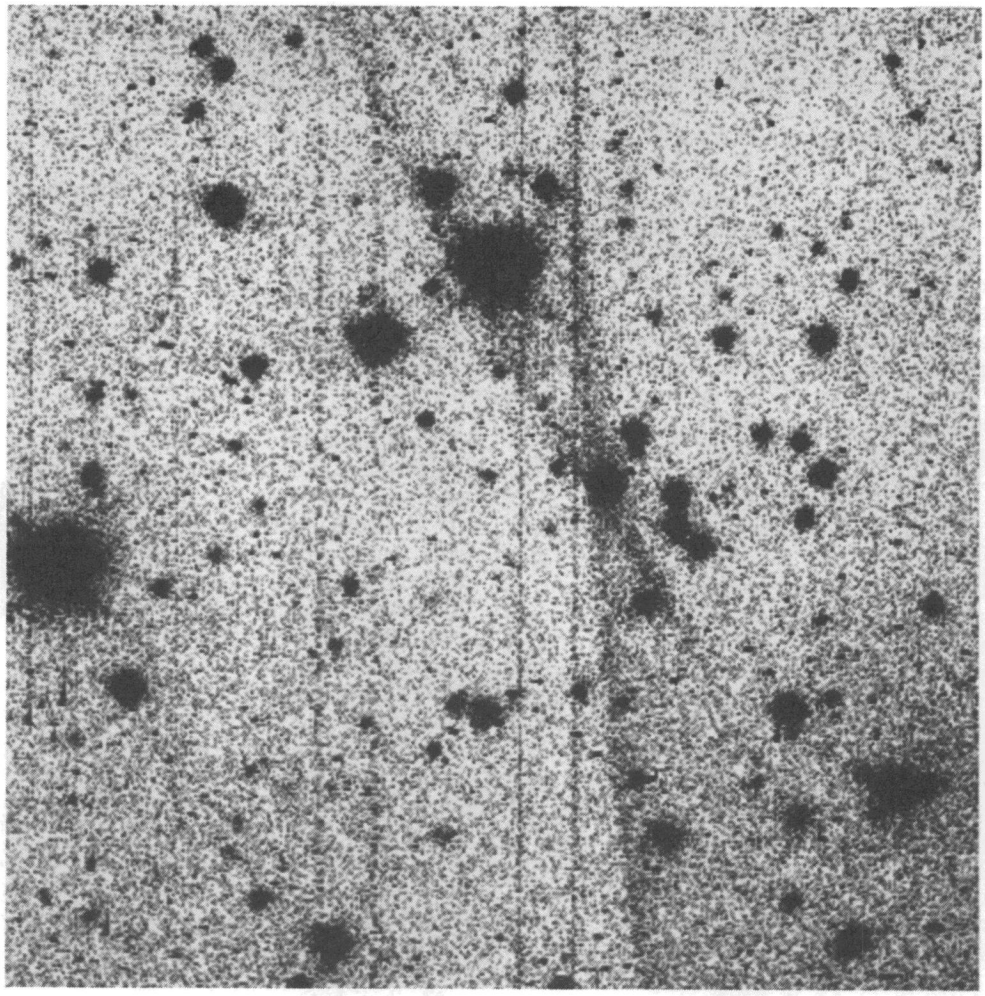

FIG. 9.—Deep Hα image of Balmer-dominated filaments near the Cygnus Loop southeastern knot taken at Lick Observatory. These are the crossing filaments which are just visible at the southeastern corner of the wide-field Hα image shown in Fig. 2. The field of view is 2'.4 × 2'.4. North is at the top, and east to the left.

optical knot is just the tip of a larger cloud. If the blast wave is encountering additional cloud material at this position of the brightest X-ray emission, then the size of the cloud is at least 3–4 times that of the optical knot.

The line of sight toward this X-ray "hot spot" includes the projected edge of the blast wave; therefore, this region should be correspondingly bright. By summing the X-ray brightness of typical reverse-shocked regions to the west of the southeastern knot, and the southern section of the blast wave, we can demonstrate that the superposition of two such regions along the line of sight could lead to the observed surface brightness.

A further factor may contribute to the X-ray emissivity along the southern edge of the knot. The flow of shocked gas past the southern edge of the southeastern knot will be almost tangential to the cloud surface (note the direction to the center of the remnant indicated in Fig. 7). This configuration is Kelvin-Helmholtz unstable (ignoring the magnetic field) and can lead to entrainment of shocked cloud gas into the gas behind the blast wave. If enough time has elapsed for the nonlinear growth of Kelvin-Helmholtz modes, then X-ray emissivity of the post–blast-wave gas will be enhanced. The Kelvin-Helmholtz growth time is comparable to the cloud crushing time (Klein et al. 1994). Since we have argued for a recent encounter with the cloud, this instability may not be well developed.

When viewed in Hα the southeastern knot appears asymmetric because of the prominence of the southern Balmer line filament. A combination of increased preshock density, favorable viewing angle, and high neutral H fraction probably accounts for the brightness of this Balmer line filament.

A similar picture with an X-ray–bright knot appearing downstream of a region of shear flow between the X-ray–emitting gas and a radiative shock exists in the XA region studied by Hester & Cox (1986). *Hubble Space Telescope* images of this region show the development of Kelvin-Helmholtz instabilities on the back side of the radiative shock (Hester 1995). High spatial resolution images of the southeastern knot region would help to establish the role of instabilities and entrainment of gas from the surface of the cloud.

4.4. *The Big Picture*

Our analysis emphasizes two themes which are important in current discussions of the structure of the Cygnus Loop: (1) the recency of the encounter with the blast wave and (2) the preparation of the local interstellar medium by the progenitor star during its presupernova evolution. These two concepts combine to produce a view of the Cygnus Loop as a "cavity explosion" (McCray & Snow 1979). While our discussion of the southeastern knot is apparently in accord with these ideas, it is dangerous to draw general conclusions about the Cygnus

Loop from the structure of such a small region. Further progress on the Cygnus Loop depends to a large extent on applying the results of detailed studies such as this to the large-scale X-ray, optical, and radio morphology.

5. CONCLUSIONS

High-resolution *ROSAT* X-ray data for the southeastern region of the Cygnus Loop SNR show the early stages of the interaction of the blast wave with a cloud in unprecedented detail. By combining optical and X-ray imaging it is straightforward to trace the blast wave and reflected shocks in the vicinity of the bright optical knot which first drew attention to this region. The correlation between X-ray emission and Balmer line filaments is used to trace the blast wave and allows us to resolve the difficulties in interpreting the morphology caused by projection effects. We show that the blast wave forms a continuous surface. The southeastern knot forms an indentation on this surface.

The prominence of the southeastern knot in X-ray emission is due to the overpressure ($\simeq 3$–6 times the bast wave pressure) of a reverse shock. The presence of a reverse shock requires that the blast wave has just run into a large cloud. These conclusions conflict with previous work on this region, which deduced that the southeastern knot represented the late stages of a small cloud which has been overrun by the blast wave. We review the evidence in favor of a small engulfed cloud and determine that, in the light of the new data, this view of the southeastern knot is no longer convincing.

This work was supported in part by grants from NASA and the Packard foundation. We thank Rosa González for help with observing at the Lick 40 inch telescope. N. A. L. was supported by an NSF fellowship.

REFERENCES

Aschenbach, B. 1988, Appl. Opt., 27, 1404
Bedogni, R., & Woodward, P. R. 1990, A&A, 231, 481
Bertoldi, F. 1989, ApJ, 346, 735
Charles, P. A., Kahn, S. M., & McKee, C. F. 1985, ApJ, 295, 456
Curiel, S., et al. 1995, in preparation
David, L. P., Harnden, F. R., Kearns, K. E., & Zombeck, M. V. 1993, The *ROSAT* High-Resolution Imager (Cambridge: US ROSAT Science Data Center, Smithsonian Astrophys. Obs.)
Falle, S. A. E. G., & Giddings, J. R. 1988, in Lecture Notes in Physics, 316, Supernova Shells and their Birth Events, ed. W. Kundt (Berlin: Springer), 83
Fesen, R. A., Blair, W. P., & Kirshner, R. P. 1982, ApJ, 262, 171
Fesen, R. A., Kwitter, K. B., & Downes, R. A. 1992, AJ, 104, 719
Graham, J. R., Wright, G. S., & Geballe, T. R. 1991a, ApJ, 372, L21
Graham, J. R., Wright, G. S., Hester, J. J., & Longmore, A. J. 1991b, AJ, 101, 175
Heathcote, S. R., & Brand, P. W. J. L. 1983, MNRAS, 203, 67
Hester, J. J. 1987, ApJ, 314, 187
———. 1995, in preparation
Hester, J. J., & Cox, D. P. 1986, ApJ, 300, 675
Hester, J. J., Parker, R. A. R., & Dufour, R. J. 1983, ApJ, 273, 219
Hester, J. J., & Raymond, J. C. 1988, in Supernova Remnants and the Interstellar Medium, ed. R. S. Roger & T. L. Landecker (Cambridge: Cambridge Univ. Press), 415
Hester, J. J., Raymond, J. C., & Blair, W. P. 1994, ApJ, 420, 721
Klein, R., McKee, C. F., & Colella, P. 1994, ApJ, 420, 213
Ku, W. H.-M., Kahn, S. M., Pisarski, R., & Long, K. S. 1984, ApJ, 278, 615
Landau, L. D., & Lifshitz, E. M. 1987, Fluid Mechanics (London: Pergamon), 468
McCray, R., & Snow, T. P. 1979, ARA&A, 17, 213
McKee, C. F., & Cowie, L. L. 1975, ApJ, 195, 715
McKee, C. F., & Ostriker, J. P. 1977, ApJ, 218, 148
Minkowski, R. 1958, Rev. Mod. Phys., 30, 1048
Petre, R., Canizares, C. R., Kriss, G. A., & Winkler, P. F. 1982, ApJ, 258, 22
Raymond, J. C., Hester, J. J., Cox, D. P., Blair, W. P., Fesen, R. A., & Gull, T. R. 1988, ApJ, 324, 869
Raymond, J. C., & Smith, B. W. 1977, ApJS, 35, 419
Seward, F. D. 1990, ApJS, 73, 781
Spitzer, L. 1982, ApJ, 262, 315
Stone, J. M., & Norman, M. L. 1992, ApJ, 390, L17
Zombeck, M. V., et al. 1990, Proc. SPIE, 1344, 267